nature ecology & evolution

ARTICLES

https://doi.org/10.1038/s41559-017-0431-0

Potentially dangerous consequences for biodiversity of solar geoengineering implementation and termination

Christopher H. Trisos[1*], Giuseppe Amatulli[2,3,4], Jessica Gurevitch[5], Alan Robock[6], Lili Xia[6] and Brian Zambri[6]

Solar geoengineering is receiving increased policy attention as a potential tool to offset climate warming. While climate responses to geoengineering have been studied in detail, the potential biodiversity consequences are largely unknown. To avoid extinction, species must either adapt or move to track shifting climates. Here, we assess the effects of the rapid implementation, continuation and sudden termination of geoengineering on climate velocities—the speeds and directions that species would need to move to track changes in climate. Compared to a moderate climate change scenario (RCP4.5), rapid geoengineering implementation reduces temperature velocities towards zero in terrestrial biodiversity hotspots. In contrast, sudden termination increases both ocean and land temperature velocities to unprecedented speeds (global medians >10 km yr^{-1}) that are more than double the temperature velocities for recent and future climate change in global biodiversity hotspots. Furthermore, as climate velocities more than double in speed, rapid climate fragmentation occurs in biomes such as temperate grasslands and forests where temperature and precipitation velocity vectors diverge spatially by >90°. Rapid geoengineering termination would significantly increase the threats to biodiversity from climate change.

The redistribution of species caused by climate change represents one of the greatest threats this century to biodiversity, affecting ecosystem functioning and human wellbeing[1]. Solar radiation management by the deliberate injection of aerosols into the stratosphere (hereafter 'geoengineering') could temporarily offset radiative forcing from greenhouse gases by reflecting sunlight back to space, cooling the Earth[2–5]. While geoengineering has never been tested outdoors, large volcanic eruptions provide evidence that increased stratospheric aerosols would cool the planet[6]. With greenhouse gas emissions trajectories making it unlikely that global warming will remain below 2 °C[7], geoengineering is receiving increased research and policy attention as a tool to limit anthropogenic climate change and buy time for additional climate mitigation and adaptation efforts[2–4,8]. The technical capacity to execute sulphur aerosol injection is relatively advanced compared to other climate engineering schemes[4,9], the estimated direct economic costs are low[3,4] and decisions on the governance of geoengineering are already being made[8]. However, the indirect costs of geoengineering are not well known. In particular, the biodiversity and ecosystem impacts of geoengineering are almost completely unexplored[5,10,11]. Given the recent increased attention on geoengineering, it is essential to evaluate the technology's potential ecological impacts to enable informed policymaking to reduce environmental risks from climate change[3].

Geoengineering could be implemented and terminated either gradually or rapidly. Here we have chosen to investigate a scenario with both rapid implementation and termination to explore the upper bound of the exposure of biodiversity to climate change impacts at either end of a geoengineering deployment. Rapid implementation is plausible, as one or a small number of nations could take action given the current lack of regulatory constraints[12,13]. Rapid termination is also feasible given the weakness of the global climate regulatory regime[8,12,13]. Interstate conflict could cause geoengineering to fail, and unintended negative consequences or regionally severe climate events such as extreme droughts could force rapid termination, even if direct attribution of these events to geoengineering could not be demonstrated[3,8,13,14]. Scholars of climate politics and policy have noted that the challenge of sustaining the climate-change-offsetting effects of geoengineering and the risks of termination are a serious concern regarding the deployment of geoengineering[8,12–14] (but see ref. [15]). Furthermore, the concomitant rapid climate changes[16] (Fig. 1) represent potentially the most significant and yet also unexplored consequences for biodiversity and ecosystems from geoengineering[5].

As climate changes, the appropriate conditions necessary for the persistence of a species move across the Earth, driving species' geographic range movements in response to climate change[17,18]. Indeed, species that fail to track moving climates may go extinct, despite suitable climate conditions being present elsewhere[19,20]. To this end, climate velocities—the rate of climate change through time divided by the rate across space[21,22]—quantify the speeds and directions of shifting climates and have predicted range movements for a wide variety of marine and terrestrial species[17,18]. Climate velocities thus provide a more biologically relevant metric of exposure to climate change than traditional macroclimatic anomalies, and can identify regions where species are threatened by being unable to move fast enough to track moving climates[21,23,24].

We used a 1° latitude–longitude grid to compare climate velocities for the Geoengineering Model Intercomparison Project

[1]National Socio-Environmental Synthesis Center, University of Maryland, Annapolis, MD, USA. [2]School of Forestry & Environmental Studies, Yale University, New Haven, CT, USA. [3]Center for Research Computing, Yale University, New Haven, CT, USA. [4]Center for Science and Social Science Information, Yale University, New Haven, CT, USA. [5]Department of Ecology and Evolution, Stony Brook University, Stony Brook, NY, USA. [6]Department of Environmental Sciences, Rutgers University, New Brunswick, NJ, USA. *e-mail: ctrisos@sesync.org

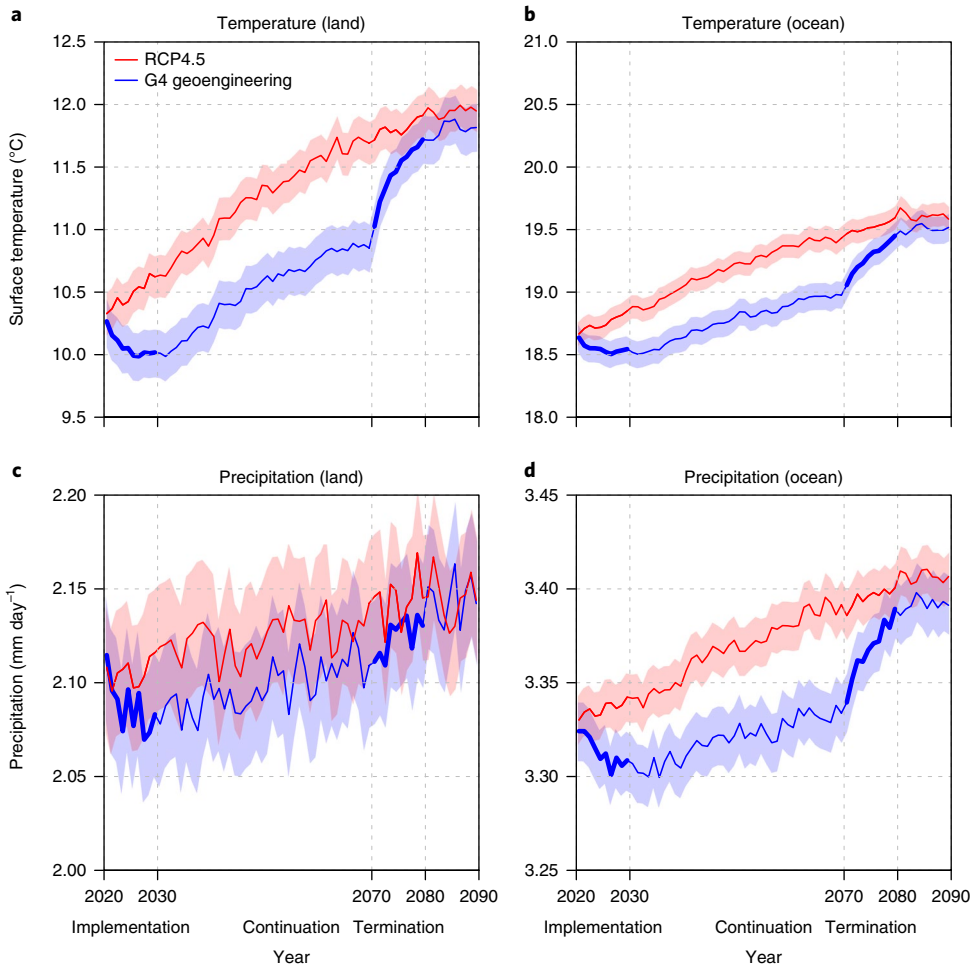

Fig. 1 | Global mean temperature and precipitation for the Geoengineering Model Intercomparison G4 scenario (solar geoengineering) and RCP4.5. **a**, Surface air temperature. **b**, Sea surface temperature. **c**, Daily precipitation on land. **d**, Daily precipitation over the ocean. Lines show the multi-model average across four climate models, each with three ensemble members. Bold lines show the climate response for the ten-year periods following sudden geoengineering implementation and termination. Shaded areas show one standard deviation above and below the multi-model average of the 12 ensemble members.

(GeoMIP) G4 scenario[25] to representative concentration pathway 4.5 (RCP4.5)[26], an intermediate emissions climate change scenario without geoengineering. We also compared G4 geoengineering to historical climate data (1960–2014). In G4, geoengineering begins in 2020 with an injection of 5 Tg SO_2—equivalent to a quarter of the 1991 Pinatubo Mountain volcanic eruption—into the stratosphere at the Equator, which is then continued annually until being terminated abruptly in 2070. This results in approximately equal sulphur injections to the Northern and Southern Hemispheres. We selected the G4 scenario because it posits that geoengineering is used only to partially offset increases in radiative forcing from RCP4.5, in which CO_2 emissions peak around 2040, making it both more credible and conservative than other GeoMIP scenarios[25].

Results and discussion

Global cooling from rapid geoengineering implementation (Fig. 1a,b) results in temperature velocity vectors with the opposite direction to warming (that is, negative velocities) that have especially high speeds in polar regions and the Indo-Pacific Ocean (Fig. 2a). In contrast, the Amazon Basin, eastern Pacific, Alaska and the Weddell Sea have high positive temperature velocities from warming, in agreement with known patterns of increased probability of El Niño following large volcanic eruptions[27,28]. For the many species already closely tracking positive climate velocities for recent warming[17,18] (Fig. 2c), the rapid switch from positive to negative velocities with geoengineering implementation would be expected to halt or even reverse climate-driven range shifts. In contrast, where species-range shifts have lagged past climate warming, the impact of large negative temperature velocities associated with cooling would be reduced and could be beneficial[29]. However, the strong decadal-scale climate variability from rapid implementation (Fig. 1) would lead to repeated switching of the climate signal (warming–cooling–warming), and such variability is known from stochastic population biology theory to negatively affect population persistence[30], increasing the risk of local extinctions.

Sudden termination of geoengineering causes extremely rapid temperature velocities (Fig. 2b) with the predicted median velocity on land (10.4 km yr^{-1}) more than four times greater, and the median ocean velocity (12.8 km yr^{-1}) more than six times greater than recent climate change (Fig. 2c and Supplementary Table 1). Temperature velocities at termination also far exceed those predicted for future climate change without geoengineering (Fig. 2d). Compared to RCP4.5, the predicted median increase in the migration speed required for species to track moving temperatures is 8.0 km yr^{-1} in the ocean and 6.4 km yr^{-1} on land, which represent 2.7- and 2.8-fold increases, respectively. The most rapid velocities

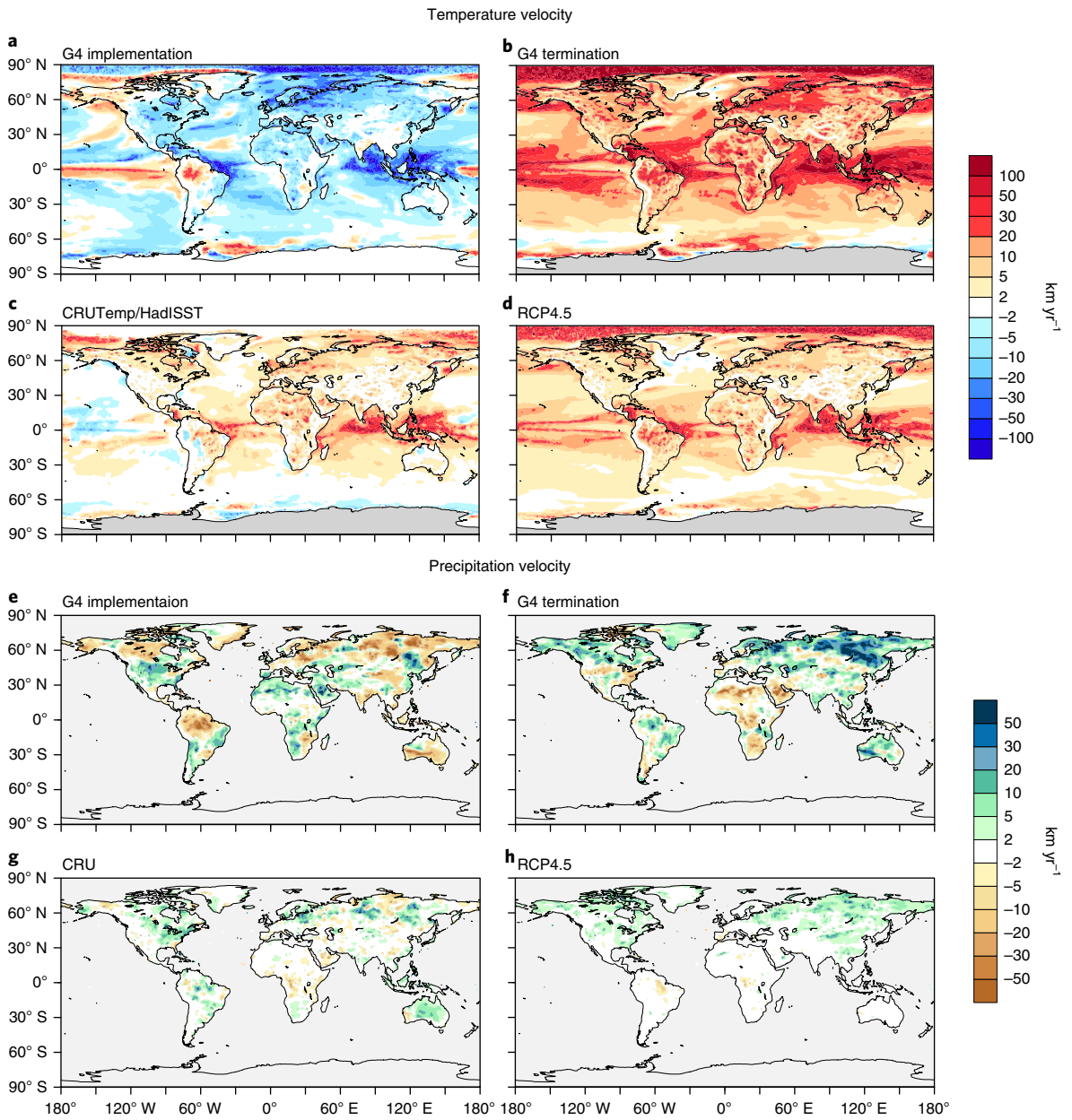

Fig. 2 | Temperature and precipitation velocities for geoengineering implementation, termination, historical climate and RCP4.5. a–**d**, Temperature velocities. **e**–**h**, Precipitation velocities. In **c**,**g**, the historical observations for 1960–2014 are shown (CRU TS3.23 for land and HadISST 1.1 for oceans). The speed (km yr^{-1}) of shifting temperature and precipitation isoclines is the same for positive and negative velocities of equal magnitude. The sign of the velocity indicates a trend of local warming (+) or cooling (−) for temperature, and wetting (+) or drying (−) for precipitation. A change of sign between scenarios represents a 180° change in the direction of climate movement (for example, from poleward to equatorward or, in mountain regions, from upslope to downslope).

occur where temperature changes are high and spatial gradients in temperature are low. Temperature velocities at termination are most extreme in tropical oceans, the biodiversity-rich Amazon Basin, Africa, Eurasia and polar regions.

At the global scale, the differences between geoengineering and RCP4.5 are less for precipitation than for temperature (Fig. 1). This is partly because, compared to temperature, precipitation velocities show much stronger differences among regions in their response (positive or negative) to each phase of geoengineering (Fig. 2e,f and Supplementary Fig. 1). Given these strong regional differences, the predicted median velocity of precipitation on land for implementation is −0.5 km yr^{-1}, indicative of the relatively weak global drying trend. Precipitation velocities for termination show a reversed pattern to implementation, and are only weakly correlated with temperature velocities for termination ($r = 0.09$). Sudden implementation reduces precipitation with high negative velocities in the Amazon, northern Europe and Asia, Australia and southeast Africa (Fig. 2h). This El Niño-like drying and warming would be likely to increase the incidence and intensity of pan-tropical forest fires (as in true El Niños), increasing CO_2 emissions and decreasing air quality, with negative impacts on public health and biodiversity[31,32].

Temporal trends in temperature and precipitation over ten-year periods, and the resulting velocities of climate change, are more variable than for longer time periods. This is because ten-year trends are more strongly influenced by sub-decadal temperature fluctuations and the phase of phenomena such as the El Niño/

Southern Oscillation. Therefore, we tested whether climate velocities for the ten-year periods following implementation (2020–2029) and termination (2070–2079) of geoengineering are predicted to exceed climate velocities for all ten-year intervals in both the historical record and in RCP4.5 climate forecasts. The median for global ocean temperature velocity for both implementation and termination is predicted to exceed the most extreme temperature velocities for all ten-year intervals in the recent historical record (Fig. 3a). Furthermore, the probability of predicted ten-year ocean temperature velocities for RCP4.5 being below the median for termination is high (0.95). Similarly, for temperature velocities on land, median velocity projections for both implementation and termination are more extreme than in the historical record (Fig. 3b). The probability of predicted RCP4.5 velocities being less than the median for termination is 0.90. In all cases for temperature, the extremes of global temperature velocity projections for implementation and termination are at least 10 km yr^{-1} greater than RCP4.5 on the same ten-year timescales. In contrast, differences between global estimates of precipitation velocity for geoengineering and for ten-year windows for either historical data or RCP4.5 forecasts are much less pronounced (Fig. 3c), which is indicative of greater variability in the precipitation response to geoengineering (Figs. 1 and 2).

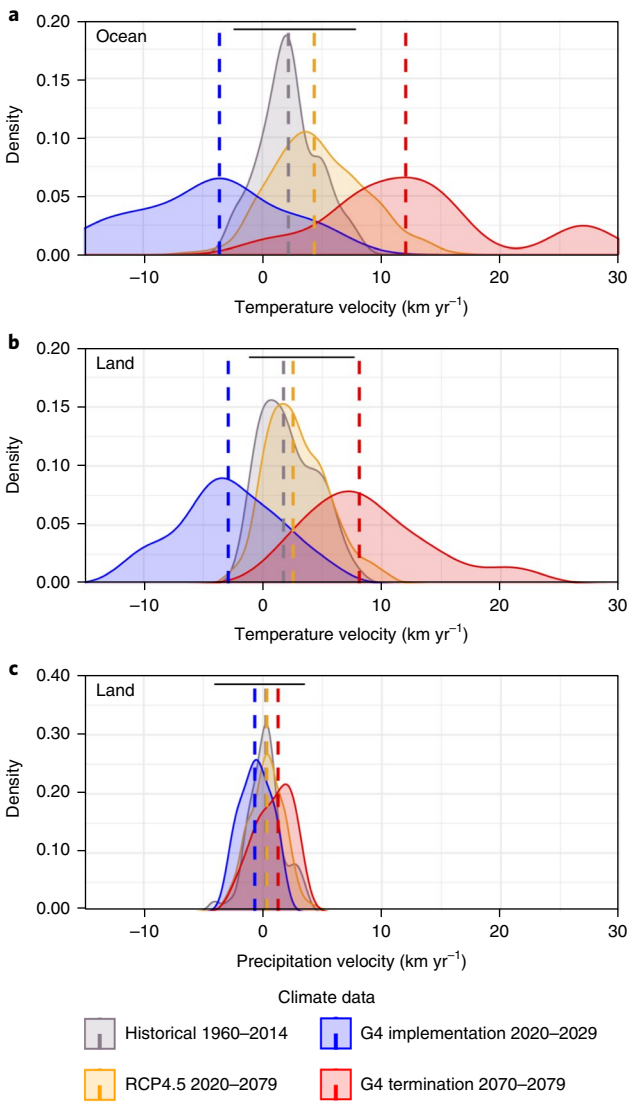

Fig. 3 | Kernel density estimates of global land and ocean climate velocities. a, Ocean temperature velocities. **b**, Land temperature velocities. **c**, Land precipitation velocities. Shown are probability density functions derived from global median velocity estimates for all ten-year moving windows within each climate data period (see Methods). Dashed lines show medians. Black horizontal bars display the range of observed climate velocities in historical data (CRU TS3.23 for land and HadISST 1.1 for oceans). The sign of the velocity value indicates the global climate trend of warming (+) or cooling (−) for temperature, and wetting (+) or drying (−) for precipitation. The speed (km yr^{-1}) is the same for positive and negative velocities of equal magnitude.

The average of the speed component of temperature and precipitation velocity (that is, climate displacement) is predicted to be faster for geoengineering termination than for RCP4.5 for more than 90% of the land and ocean. Thus, to better identify regions most affected by sudden termination when compared to climate change with no geoengineering, we mapped climate displacement for termination against RCP4.5 (Fig. 4a). Tropical ocean regions and the Arctic are predicted to have high climate displacement under both scenarios. However, compared to RCP4.5, an additional 32% of Earth's surface is predicted to be exposed to high climate displacement (>10 km yr^{-1}) from sudden termination (red regions in Fig. 4a), notably subtropical and northern temperate oceans, and much of North America, Africa and Eurasia. These regions are expected to face the most significant increases in local extinction risk from sudden termination as species fail to track faster moving climates.

Distinctive ecological assemblages or biomes are often associated with particular combinations of temperature and precipitation[33,34]. Understanding where sudden termination is predicted to cause both large and spatially divergent temperature and precipitation velocities (climate fragmentation) is therefore useful for assessing impacts on ecological communities. At the biome scale, temperature velocities for termination are highest in tundra, boreal forests, temperate grasslands and tropical biomes (medians >10 km yr^{-1}), and lowest in montane-associated biomes, owing to topographic effects (Supplementary Fig. 3). At termination, 29% of the land surface has temperature and precipitation velocity vectors that diverge by >90° and more than double in speed compared to RCP4.5 (Fig. 4b). Temperate grasslands, temperate forests and Mediterranean-type biomes are most exposed to this increased speed of climate fragmentation (Supplementary Table 2). In these regions, a more rapid divergence in temperature and precipitation conditions could increase local extinction probabilities as species climate niches fragment[35], and accelerate changes in biome boundaries and ecosystem function by driving the rapid disassembly of ecological communities as temperature- and precipitation-dependent species are forced rapidly in different directions to track climate change[36].

Most of Earth's biodiversity resides in the tropics (Fig. 5a). Rapid geoengineering implementation drives large negative temperature velocities for tropical marine biodiversity hotspots (Fig. 5c), potentially reversing range shifts and providing relief to heat-stressed taxa such as corals[29]. On land, implementation drives negative precipitation velocities (Fig. 5b) and reduces temperature velocities to close to zero for biodiversity hotspots, mitigating warming-induced range movements (Fig. 5d). In contrast, as geoengineering continues, temperature velocities for G4 are similar to RCP4.5 (Fig. 5c,d and Supplementary Figs. 4 and 5) even as temperature increases are offset (Fig. 1). For tropical species with narrow thermal tolerances, even relatively small amounts of warming threaten species survival[35]. Thus, for G4 levels of solar radiation management with CO_2 emissions at the same rate as RCP4.5, the offset in climate-induced migration would be short-lived (decades), after which dispersal rates to keep pace with climate change are predicted to be similar for G4 and RCP4.5.

Across terrestrial and marine biodiversity hotspots, sudden termination results in extreme temperature velocities that are 2–4 times faster than those for either historical data or future climate change

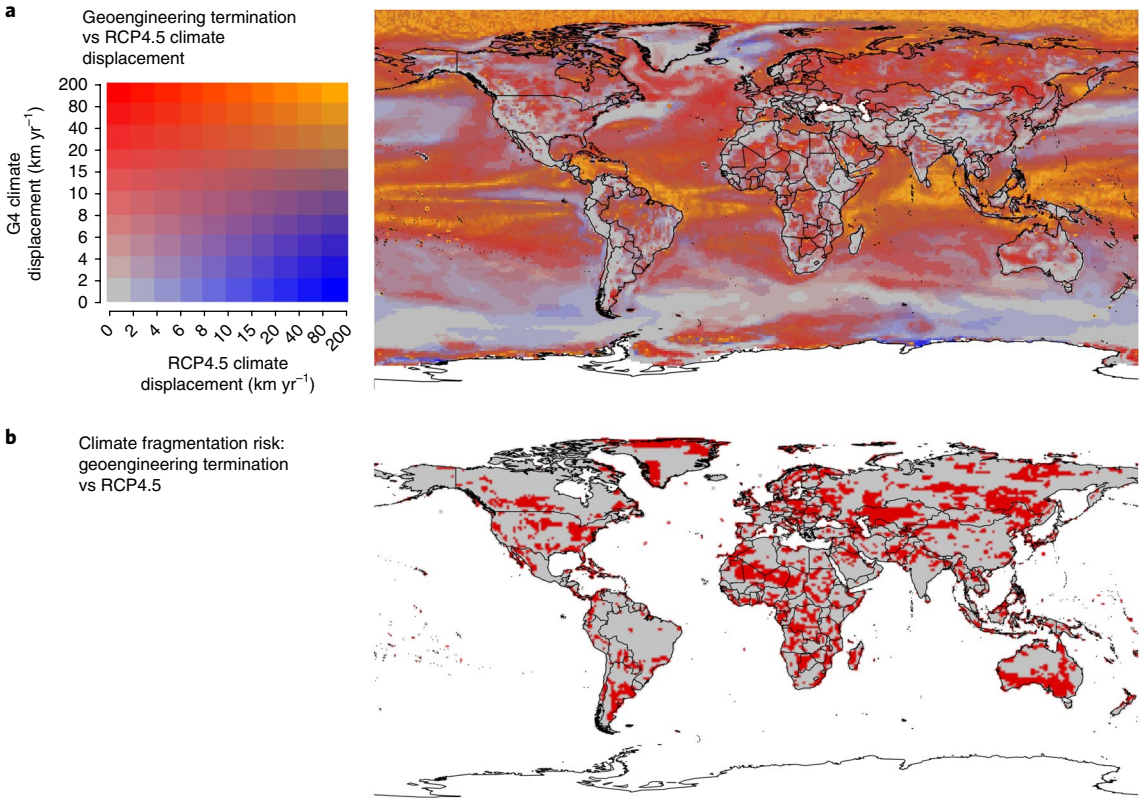

Fig. 4 | Climate displacement and fragmentation from sudden geoengineering termination. a, Climate displacement for terrestrial regions is the average speed of temperature and precipitation velocities, whereas marine regions show only the speed of temperature velocity. Red regions, where predicted climate displacement is low for RCP4.5 but high for termination, are a particular concern for increased local extinction risk with termination. **b**, Relative increase in climate fragmentation risk with sudden termination. Red indicates regions that are both (1) where G4 termination velocity speeds for both temperature and precipitation are double or more than double RCP4.5, and (2) where G4 termination velocities for temperature and precipitation diverge in direction by >90°.

without geoengineering, and are highest in tropical marine environments (medians >38 km yr^{-1}; Fig. 5c,d and Supplementary Table 1). High temperature velocities in tropical regions may result from smaller temperature increases at termination than for high latitudes, being divided by shallower spatial gradients in temperature (Fig. 2 and Supplementary Figs. 2,6). Thus, the effect of high temperature velocities on biodiversity could be partly mitigated if many species are far from their upper thermal limits. However, tropical species generally have narrower thermal tolerances than their temperate counterparts and are often near or above optimal temperatures, making climate tracking more important for their survival[37–39]. Extreme climate velocities from geoengineering termination thus represent a potentially acute threat to species survival in the most biodiverse regions on Earth.

Mean estimates of species-range movements in response to recent warming for arthropods, birds, fish, reptiles and mammals (1.7 km yr^{-1})[18] are 4–7 times slower than predicted temperature velocities from sudden termination. Furthermore, in a broad sample of mammals, the median temperature velocity from termination in mammal biodiversity hotspots (9.8 km yr^{-1}) is faster than the median dispersal rate for 93% of species and faster than the maximum dispersal rate for a majority of species[19] (Supplementary Fig. 7). Given that mammals have relatively high dispersal ability, this result suggests that less dispersive taxa may be even more at risk of extinction. Indeed, the association of regions of low endemism with high climate velocity since the Last Glacial Maximum has been shown to be strongest for poorly dispersing amphibian taxa, indicative of increased extinctions when poorly dispersing species fail to track climate change[23]. Thus, while differences in climate velocity between terrestrial hotspots for some taxa are small, that amphibian biodiversity hotspots have the highest temperature velocities from sudden termination suggests that increased extinction risks would be especially severe for this group (Fig. 5c). Further work is needed to link climate velocities with species-specific dispersal rates and future dispersal cost pathways to obtain more detailed estimates of possible extinctions, in order to improve forecasts of the consequences of geoengineering for biodiversity.

We assessed biodiversity impacts using the G4 geoengineering scenario. However, our results are informative for any sudden geoengineering implementation or termination. The amplitude of the climate response depends on the imbalance between climate forcing from increased greenhouse gases and the geoengineering forcing implemented[25]. The size of the climate shocks described here could occur earlier or be even greater if we choose to continue business-as-usual CO_2 emissions, better represented by the more severe RCP8.5 scenario, or if a larger SO_2 injection was employed.

Given current emissions trajectories, it would be irresponsible not to study the potential benefits and costs of proposed climate engineering[3,5,8,10]. Aggressive emissions cuts remain the most robust way to reduce biodiversity impacts from climate change. However, as society considers geoengineering to reduce climate impacts, the results presented here call for continued research into the ecological consequences of geoengineering and extreme caution in the development of policy and governance mechanisms that mitigate the ecological risks of rapid geoengineering implementation and termination.

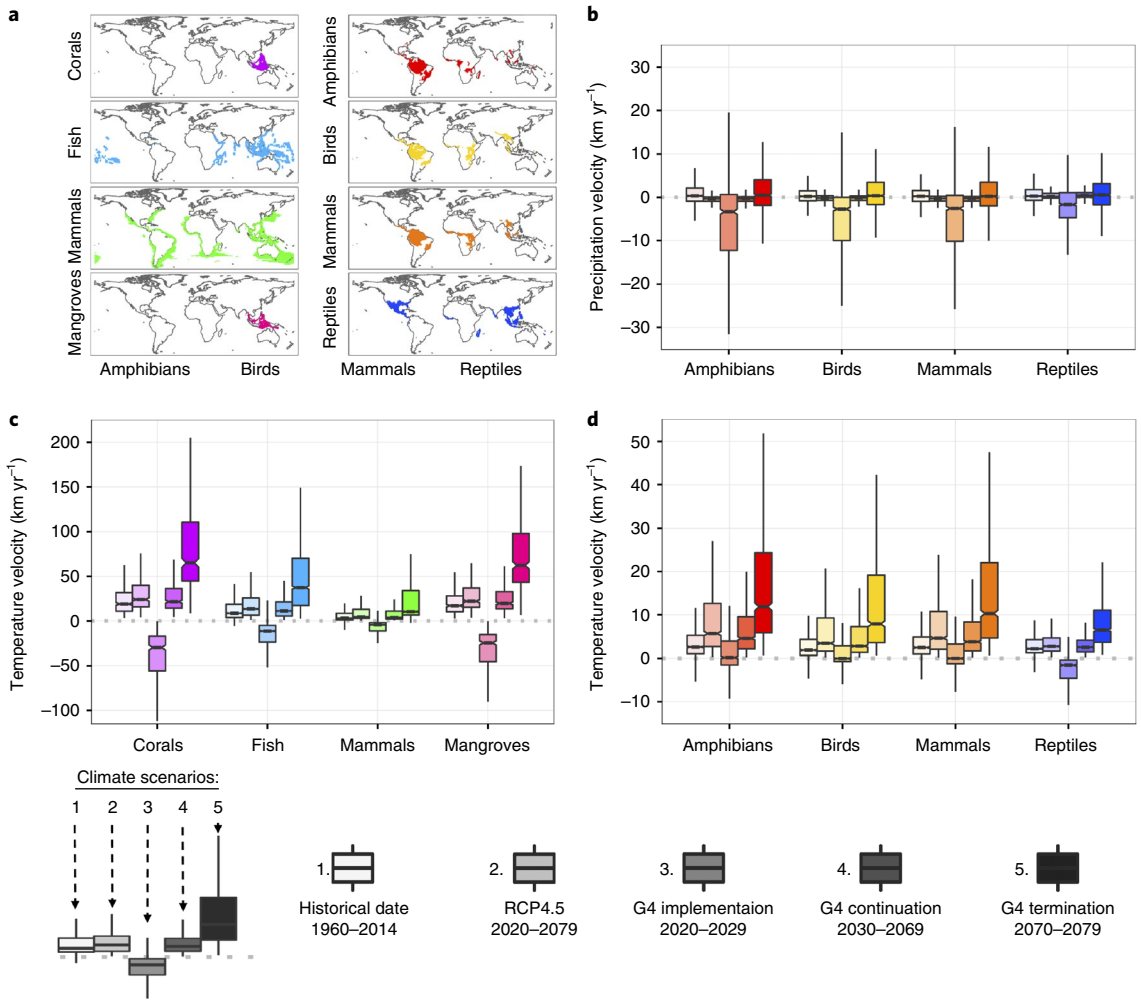

Fig. 5 | Climate velocities for global biodiversity hotspots for historical climate, RCP4.5 and geoengineering. a, The locations of terrestrial and marine biodiversity hotspots, which are the top 10% most species-rich areas where a given taxonomic group is found. **b**, Precipitation velocities for terrestrial biodiversity hotspots. **c**, Temperature velocities for marine biodiversity hotspots. **d**, Temperature velocities for terrestrial biodiversity hotspots. Note different scales on the y axis. The sign of the velocity value indicates local warming (+) or cooling (-) for temperature, and wetting (+) or drying (-) for precipitation. Boxplots show the median, first and third quartiles for climate velocity for each hotspot and climate scenario. Lines show minimum and maximum values. Box colour indicates the biodiversity hotspot. Box shading indicates specific climate scenarios (detailed at the bottom of the figure).

Methods

Climate observations and simulations. We used projections of near-surface air temperature, sea surface temperature and precipitation from four climate models (Supplementary Table 3) developed for GeoMIP, each of which included RCP4.5 forcing for 2006–2100 and for G4 experiments. Some earlier geoengineering experiments used unreasonable global warming forcing or merely turned down the solar constant. Instead, the G4 scenario of GeoMIP followed two previous climate models[40,41] and simulated the more 'realistic' creation of a stratospheric aerosol layer. The G4 scenario posited that, beginning in 2020, the same increased radiative forcing as for the RCP4.5 scenario is partially offset by a constant negative forcing from a stratospheric aerosol cloud produced by an annual injection of 5 Tg SO_2 into the lower stratosphere over the Equator. After 50 years of geoengineering, the G4 experiments terminate this sulphate aerosol injection. The simulations are then continued from 2070 for at least a further 20 years, so that the post-engineered rebound of the climate system could be assessed. The G4 scenario results in approximately equal sulphur injections to the Northern and Southern Hemispheres. Different scenarios that concentrate aerosols in a single hemisphere would result in different climate responses[42].

We used all model results available for the RCP4.5 and G4 experiments from GeoMIP to avoid being dependent on any single climate model. Following standard practice in climate modelling, we used three ensemble members (that is, simulations beginning with slightly different initial conditions) from each of the four climate models to account for natural variability of the climate system, allowing evaluation of the extent to which the results are forced (controlled by the climate boundary conditions) or random.

Historical sea surface temperatures for the period 1960–2014 were obtained from the Hadley Centre HadISST v1.1 dataset as monthly 1° grids[43]. Historical precipitation and land surface temperature for the period 1960–2014 were obtained as 0.5° grids from the Climate Research Unit TS3.23 dataset[44].

Global climate trends with geoengineering. To produce Fig. 1, we first performed a bias correction by adjusting each RCP4.5 and G4 simulation using the differences between the overall mean of RCP4.5 and the mean of RCP4.5 for each model. Second, we detrended the curves to calculate the standard deviation among the 12 ensemble members, three from each model. For the RCP4.5 curves, the upward trend was taken over the 70 years; for the G4 curves, we separated the curves into two segments to detrend, 50 years of geoengineering and 20 years after geoengineering. Standard deviations were calculated with respect to the detrended curves. Finally, we calculated the average of temperature or precipitation among the models, and added or subtracted one standard deviation (calculated with each ensemble member of each model) to get the upper and lower boundaries of the envelopes. This shows that at the global scale the geoengineering-induced climate responses are robust to differences among climate models and to the natural variability of the climate system (Fig. 1).

Climate velocity calculations. We separated G4 model outputs into the 'implementation' period (the first 10 years of SO_2 injection, 2020–2029); the 'continuation' period (2030–2069); and the 'termination' period (the 10 years after sudden termination of SO_2 injection, 2070–2079) (Fig. 1). Because it takes approximately two years following the beginning or end of SO_2 injection to

produce either an equilibrium sulphate aerosol cloud or a clean stratosphere[45], and because the upper ocean, which responds quickly to radiative forcing, has an approximately seven-year *e*-folding time for responding[46], 10 years is a reasonable period to study the climate transitions. Moreover, implementation and termination are critical periods for which to calculate the speed and direction of shifting climate contours because 10 years of large and rapid climate change would provide very little opportunity for evolutionary responses as opposed to species migration to buffer the survival of many taxa.

We calculated climate velocities using a 1° latitude–longitude grid of temperature and precipitation, a spatial grain that enables global-scale inference while still capturing the influence of topography on climate velocity[22]. All analyses used mean annual temperature (°C) and total annual precipitation (mm). Climate velocities were calculated by dividing temporal trends in precipitation (mm yr^{-1}; Supplementary Fig. 1) and temperature (°C yr^{-1}; Supplementary Fig. 2) by the spatial gradients in their observed long-term averages (mm km^{-1} and °C km^{-1}; Supplementary Fig. 7)[21,22].

Spatial gradients in climate variables were calculated on a 1° grid using the long-term averages for mean annual temperature and annual precipitation over the historical data period 1960–2014. To better capture transitions from sea ice to ocean with climate warming, instead of removing months with sea ice from calculations of mean annual temperature for a grid cell, as has been done in previous studies[11], in both climate model and historical data we set sea ice to −1.8 °C before calculating temporal trends or spatial gradients. To reduce the occurrence of flat spatial gradients that cause infinite velocities (following ref. [21]) we added uniformly distributed random noise to the long-term average for every grid cell—distributed from −0.05 to 0.05 °C for temperature and 0.001 to 0.1 mm for precipitation—before calculating spatial gradients. We removed from our analyses isolated, individual grid cells such as small oceanic islands for which spatial gradients to neighbouring cells could not be calculated. The spatial gradient and direction (that is, the slope aspect) for each grid cell were calculated from a neighbourhood of 3 × 3 grid cells following the convention that vectors point from high to low values for a climate variable. Therefore, vectors of climate velocity point in the same direction as the slope aspect of a climate variable when the temporal trend for that variable is increasing, but are opposite in direction when the temporal trend is negative. Divergence in temperature and precipitation was calculated as the angle between the temperature and precipitation velocity vectors[36].

We calculated temporal trends for historical precipitation and temperature at 0.5° resolution and then regridded to 1° by averaging across 2 × 2 neighbourhoods. This was done to match the 1° spatial resolution for observed sea surface temperature, allowing for comparison of land and ocean climate velocities. All GeoMIP climate model data were regridded to a 1° grid using a bilinear interpolation method[47] before calculating temporal trends and climate velocities.

Temporal trends in temperature and precipitation, and the resulting velocity of climate change, are much more variable over ten-year periods than over longer periods, mostly because the ten-year trends are strongly influenced by sub-decadal temperature fluctuations and the phase of phenomena such as the El Niño/Southern Oscillation. Thus, we tested whether the predicted effects of geoengineering implementation (2020–2029) and termination (2070–2079) on climate velocities exceeded natural and projected climate fluctuations on the same timescales by comparing the probability density functions for climate velocities for the ten-year implementation and termination periods with those for all ten-year intervals in historical data records and RCP4.5 climate forecasts. To do this, we used linear regression to calculate a temporal trend for temperature and precipitation for the ten years of implementation and termination, as well as every ten-year moving window interval in the longer G4 continuation, RCP4.5 and historical data time periods (for example, RCP4.5 ten-year periods were: 2020–2029, 2021–2030... 2069–2078, 2070–2079). We calculated these ten-year trends for each of the three ensemble members in each of the four GeoMIP models for RCP4.5 and G4, and for the single record of historical data. We divided each ten-year trend by the spatial gradient from the historical data to calculate a climate velocity for every ten-year interval. Thus, the resulting number of ten-year climate velocity estimates for each climate period was a multiple of the number of ensemble members, models and ten-year intervals: $n = 12$ for G4 implementation (2020–2029); $n = 12$ for G4 termination (2070–2079); $n = 372$ for G4 continuation (2030–2069); $n = 612$ for RCP4.5 (2020–2079); and $n = 46$ for historical data (1960–2014). We calculated a global median for each climate velocity estimate and estimated probability density functions of the global medians for each climate period using a Gaussian kernel density estimator in R. We used medians weighted by area for all global estimates of climate velocity to account for differences in area among 1° grid cells (smaller grid cells at high latitudes). For a given time period and scenario (for example, G4 termination 2070–2079 or RCP4.5 2020–2079), we mapped climate velocities as the grid cell averages of all constituent ten-year climate velocity estimates and mapped uncertainty as the standard deviation (Supplementary Figs. 8 and 9). These mapped averages were used for further biodiversity hotspot and biome analyses.

Climate velocities for RCP4.5 and the G4 continuation period were very similar, making the predicted differences in climate velocities as the climate shifts from G4 continuation to G4 termination very similar to the differences predicted between RCP4.5 and G4 termination (Supplementary Figs. 4 and 5).

Biodiversity hotspots and biome analyses. Marine and terrestrial biodiversity hotspots were defined as the top 10% most species-rich areas on Earth where a given taxon is found[48], and were delimited for eight different terrestrial (reptiles, mammals, birds and amphibians) and marine (mangroves, mammals, fish and corals) taxonomic groups. We used expert-verified range maps[49,50] to count the number of species with ranges that overlapped each cell in an equal-area grid with a resolution of 100 km. We rasterized species-range maps at a resolution of 0.25° to minimize the border effect, and then averaged to a 100 km equal-area grid. We then selected the 10% most species-rich cells for each taxonomic group using only those cells that had species present for the given group. Climate velocities were interpolated to the equal-area grid using an area-weighted average interpolation. We used biomes from the World Wildlife Fund Terrestrial Ecoregions[51]. Climate velocity estimates for biomes were obtained by overlaying climate velocity grids at 1° resolution with biomes and extracting area-weighted climate velocity values.

Code availability. The code for calculating climate velocities is available at https://github.com/selvaje/YaleRep/blob/master/GEOING/sc2_temporal_slope_observation_after_review.sh and https://github.com/selvaje/YaleRep/blob/master/GEOING/sc3_temporal_slope_models_after_review.sh

Data availability. The climate data used in this paper and the derived global climate velocities are publicly available online at http://people.envsci.rutgers.edu/bzambri/wwwfiles/climate_velocities/. Species geographic range maps are available at http://www.iucnredlist.org/technical-documents/spatial-data and http://datazone.birdlife.org

Received: 11 May 2017; Accepted: 28 November 2017;

References

1. Pecl, G. et al. Biodiversity redistribution under climate change: impacts on ecosystems and human well-being. *Science* **355**, eaai9214 (2017).
2. Crutzen, P. Albedo enhancement by stratospheric sulfur injections: a contribution to resolve a policy dilemma? *Clim. Change* **77**, 211–219 (2006).
3. National Research Council. *Climate Intervention: Reflecting Sunlight to Cool Earth* (National Academies Press, Washington DC, 2015).
4. Keith, D. W. & MacMartin, D. G. A temporary, moderate and responsive scenario for solar geoengineering. *Nat. Clim. Change* **5**, 201–206 (2015).
5. McCormack, C. G. et al. Key impacts of climate engineering on biodiversity and ecosystems, with priorities for future research. *J. Integr. Environ. Sci.* **13**, 103–128 (2016).
6. Robock, A., MacMartin, D. G., Duren, R. & Christensen, M. W. Studying geoengineering with natural and anthropogenic analogs. *Clim. Change* **121**, 445–458 (2013).
7. Peters, G. P. et al. The challenge to keep global warming below 2 °C. *Nat. Clim. Change* **3**, 4–6 (2013).
8. *Geoengineering in Relation to the Convention on Biological Diversity: Technical and Regulatory Matters* CBD Technical Series No. 66 (Secretariat of the Convention on Biological Diversity, Montreal, 2012).
9. Keith, D. W., Weisenstein, D. K., Dykema, J. A. & Keutsch, F. N. Stratospheric solar geoengineering without ozone loss. *Proc. Natl Acad. Sci. USA* **113**, 14910–14914 (2016).
10. Irvine, P. J. et al. Towards a comprehensive climate impacts assessment of solar geoengineering. *Earth's Future* **5**, 93–106 (2017).
11. Williamson, P. & Bodle, R. *Update on Climate Geoengineering in Relation to the Convention on Biological Diversity: Potential Impacts and Regulatory Framework* CBD Technical Series No. 84 (Secretariat of the Convention on Biological Diversity, Montreal, 2016).
12. Victor, D. G. On the regulation of geoengineering. *Oxf. Rev. Econ. Policy* **24**, 322–336 (2008).
13. Horton, J. B. & Reynolds, J. L. The international politics of climate engineering: a review and prospectus for international relations. *Int. Stud. Rev.* **18**, 438–461 (2016).
14. Victor, D. G., Morgan, M. G., Apt, J., Steinbruner, J. & Ricke, K. The geoengineering option: a last resort against global warming? *Foreign Aff.* **88**, 64–76 (2009).
15. Reynolds, J. L., Parker, A. & Irvine, P. Five solar geoengineering tropes that have outstayed their welcome. *Earth's Future* **4**, 562–568 (2016).
16. Jones, A. et al. The impact of abrupt suspension of solar radiation management (termination effect) in experiment G2 of the Geoengineering Model Intercomparison Project (GeoMIP). *J. Geophys. Res. Atmos.* **118**, 9743–9752 (2013).
17. Pinsky, M. L., Worm, B., Fogarty, M. J., Sarmiento, J. L. & Levin, S. A. Marine taxa track local climate velocities. *Science* **341**, 1239–1242 (2013).
18. Chen, I. C., Hill, J. K., Ohlemüller, R., Roy, D. B. & Thomas, C. D. Rapid range shifts of species associated with high levels of climate warming. *Science* **333**, 1024–1026 (2011).

19. Schloss, C. A., Nuñez, T. A. & Lawler, J. J. Dispersal will limit ability of mammals to track climate change in the Western Hemisphere. *Proc. Natl Acad. Sci. USA* **109**, 8606–8611 (2012).
20. Corlett, R. T. & Westcott, D. A. Will plant movements keep up with climate change? *Trends Ecol. Evol.* **28**, 482–488 (2013).
21. Loarie, S. R., Duffy, P. B., Hamilton, H., Asner, G. P., Field, C. B. & Ackerly, D. D. The velocity of climate change. *Nature* **462**, 1052–1055 (2009).
22. Burrows, M. T. et al. The pace of shifting climate in marine and terrestrial ecosystems. *Science* **334**, 652–655 (2011).
23. Sandel, B. et al. The influence of Late Quaternary climate-change velocity on species endemism. *Science* **334**, 660–664 (2011).
24. Burrows, M. T. et al. Geographical limits to species-range shifts are suggested by climate velocity. *Nature* **507**, 492–495 (2014).
25. Kravitz, B. et al. The Geoengineering Model Intercomparison Project (GeoMIP). *Atmos. Sci. Lett.* **12**, 162–167 (2011).
26. Moss, R. H. et al. The next generation of scenarios for climate change research and assessment. *Nature* **463**, 747–756 (2010).
27. Maher, N., McGregor, S., England, M. H. & Sen Gupta, A. Effects of volcanism on tropical variability. *Geophys. Res. Lett.* **42**, 6024–6033 (2015).
28. Pausata, F. S. R., Karamperidou, C., Caballero, R. & Battisti, D. S. ENSO response to high-latitude volcanic eruptions in the Northern Hemisphere: the role of the initial conditions. *Geophys. Res. Lett.* **43**, 8694–8702 (2016).
29. Kwiatkowski, L. et al. Coral bleaching under unconventional scenarios of climate warming and ocean acidification. *Nat. Clim. Change* **5**, 777–781 (2015).
30. Caswell, H. *Matrix Population Models* (Wiley, Hoboken, 2001).
31. Cochrane, M. A. Fire science for rainforests. *Nature* **421**, 913–919 (2003).
32. Marlier, M. E. et al. El Niño and health risks from landscape fire emissions in southeast Asia. *Nat. Clim. Change* **3**, 131–136 (2013).
33. Whittaker, R. H. *Communities and Ecosystems* (Macmillan, New York, 1975).
34. Prentice, C. et al. A global biome model based on plant physiology and dominance, soil properties and climate. *J. Biogeogr.* **19**, 117–134 (1992).
35. McCain, C. M. & Colwell, R. K. Assessing the threat to montane biodiversity from discordant shifts in temperature and precipitation in a changing climate. *Ecol. Lett.* **14**, 1236–1245 (2011).
36. Ordonez, A., Williams, J. W. & Svenning, J. C. Mapping climatic mechanisms likely to favour the emergence of novel communities. *Nat. Clim. Change* **6**, 1104–1109 (2016).
37. Deutsch, C. A. et al. Impacts of climate warming on terrestrial ectotherms across latitude. *Proc. Natl Acad. Sci. USA* **105**, 6668–6672 (2008).
38. Tewksbury, J. J., Huey, R. B. & Deutsch, C. A. Putting the heat on tropical animals. *Science* **320**, 1296–1297 (2008).
39. Janzen, D. H. Why mountain passes are higher in the tropics. *Am. Nat.* **101**, 233–249 (1967).
40. Robock, A., Oman, L. & Stenchikov, G. Regional climate responses to geoengineering with tropical and Arctic SO_2 injections. *J. Geophys. Res.* **113**, D16101 (2008).
41. Jones, A., Haywood, J., Boucher, O., Kravitz, B. & Robock, A. Geoengineering by stratospheric SO_2 injection: results from the Met Office HadGEM2 climate model and comparison with the Goddard Institute for Space Studies ModelE. *Atmos. Chem. Phys.* **10**, 5999–6006 (2010).
42. Haywood, J. M., Jones, A., Bellouin, N. & Stephenson, D. Asymmetric forcing from stratospheric aerosols impacts Sahelian rainfall. *Nat. Clim. Change* **3**, 660–665 (2013).
43. Rayner, N. A. et al. Global analyses of sea surface temperature, sea ice, and night marine air temperature since the late nineteenth century. *J. Geophys. Res.* **108**, 4407 (2003).
44. Harris, I., Jones, P. D., Osborn, T. J. & Lister, D. H. Updated high-resolution grids of monthly climatic observations – the CRU TS3.10 Dataset. *Int. J. Climatol.* **34**, 623–642 (2014).
45. Robock, A. Volcanic eruptions and climate. *Rev. Geophys.* **38**, 191–219 (2000).
46. Hartmann, D. L *Global Physical Climatology*. 2nd edn (Elsevier, Amsterdam, 2016).
47. *CDO 2015: Climate Data Operators* (accessed December 2015); http://www.mpimet.mpg.de/cdo
48. Mora, C. et al. The projected timing of climate departure from recent variability. *Nature* **502**, 183–187 (2013).
49. *IUCN Red List* (accessed August 2016); http://www.iucnredlist.org/technical-documents/spatial-data
50. *Bird Species Distribution Maps of the World* (BirdLife International, Cambridge and NatureServe, Arlington, 2015); http://datazone.birdlife.org
51. Olson, D. M. et al. Terrestrial ecoregions of the world: a new map of life on Earth: a new global map of terrestrial ecoregions provides an innovative tool for conserving biodiversity. *BioScience* **51**, 933–938 (2001).

Acknowledgements

C.H.T. was supported by the National Socio-Environmental Synthesis Center (SESYNC) under funding received from the US National Science Foundation DBI-1052875. A.R., L.X. and B.Z. were supported by US National Science Foundation grants GEO-1240507, AGS-1430051 and AGS-1617844. We thank the climate modelling groups for making their results available and GeoMIP for organizing the experiments; the Climatic Research Unit, University of East Anglia, for temperature and precipitation data; the UK Hadley Centre for sea surface temperature data; and the International Union for the Conservation of Nature and BirdLife International for species-range maps. Much of the processing chain was implemented at Yale Center for Research Computing (YCRC), and we thank the YCRC staff. We thank T. Carleton, I. Carroll, K. Conca, C. Merrow, L. Palmer, I. Quintero and N. Upham for comments. The cross-disciplinary forums provided by an American Association for the Advancement of Science (AAAS) annual meeting and SESYNC led to the meeting of C.T., J.G. and A.R., initiating this work.

Author contributions

C.H.T., A.R. and J.G. conceived the study. C.H.T., A.R., J.G., G.A., L.X. and B.Z. designed the study. C.H.T., G.A., L.X. and B.Z. performed the analysis and drew the figures. G.A. wrote the scripting procedure for the geodata processing chain. C.H.T., A.R. and J.G. wrote the paper, with substantial contributions from all authors.

Competing interests

The authors declare no competing financial interests.

Additional information

Supplementary information is available for this paper at https://doi.org/10.1038/s41559-017-0431-0.

Reprints and permissions information is available at www.nature.com/reprints.

Correspondence and requests for materials should be addressed to C.H.T.

Publisher's note: Springer Nature remains neutral with regard to jurisdictional claims in published maps and institutional affiliations.